Evaluation of SPECT Quantification of Radiopharmaceutical Distribution in Canine Myocardium

Jianying Li, Ronald J. Jaszczak, Kim L. Greer, David R. Gilland, David M. DeLong and R. Edward Coleman

Department of Radiology and Division of Biometry, Duke University Medical Center, Durham, North Carolina

This study evaluates the quantitative accuracy of SPECT for in vivo distributions of ^{99m}Tc radiopharmaceuticals using fanbeam (FB) and parallel-beam (PB) collimators and compares uniform and nonuniform attenuation correction methods in terms of quantitative accuracy. **Methods:** SPECT quantification of canine myocardial radioactivity was performed followed by well counter measurements of extracted myocardial tissue samples. Transmission scans using a line source and an FB collimator were performed to generate nonuniform attenuation maps of the canine thorax. Emission scans with two energy windows were acquired. Images were reconstructed using a filtered backprojection algorithm, with a dual-window scatter subtraction combined with either no attenuation compensation or single iteration Chang attenuation compensation based on an uniform attenuation map ($\mu = 0.152\ cm^{-1}$) or the nonuniform transmission map. **Results:** The measured mean counts from the SPECT images were converted to radionuclide concentrations (MBq/g) using a standard source calibration and were compared with those obtained using the well counter. **Conclusion:** The experimental results demonstrate that, compared with well counter values, the in vivo distributions of ^{99m}Tc were most accurately determined in FB and PB SPECT reconstructions with nonuniform attenuation compensation, under-estimated without attenuation compensation and overestimated with uniform attenuation compensation.

Key Words: SPECT; quantification; myocardium

J Nucl Med 1995; 36:278–286

SPECT provides three-dimensional maps of in vivo radiopharmaceutical distributions. An important goal of nuclear medicine research is to make SPECT a more useful imaging modality by utilizing and improving its quantitative capabilities. Many physical factors degrade SPECT images both qualitatively and quantitatively. Among them, photon attenuation is the dominant factor affecting SPECT quantitation, and various methods have been proposed to compensate for attenuation (*1–19*). In the chest, abdomen and pelvis, the true spatial distribution of attenuation coefficients is nonuniform and several methods have been developed to compensate for nonuniform attenuation (*9–19*). These methods include both filtered backprojection reconstruction with Chang's or modified Chang's attenuation compensation with a nonuniform attenuation map (*10,14,18*) and nonuniform iterative maximum likelihood reconstruction (*9,13,14,16,19*). Methods of transmission computed tomographic (TCT) data acquisition on SPECT cameras have been developed to obtain an accurate attenuation map (*9,10,13,15–17,19–22*). These methods include both sequential and simultaneous scans. Scatter is another major factor that degrades the contrast of lesions and results in a major source of error in the quantification of radionuclide concentrations. Many methods have been proposed to compensate for scatter (*23–30*). Each scatter compensation method has its advantages and disadvantages, and even the simpler approaches probably are capable of providing an adequate compensation which is accurate to about 5%–10% for many source distributions (*28,29*).

In this study, quantitative SPECT evaluations were performed on the canine myocardium using our triple-camera system (Trionix Research Laboratories, Inc., Twinsburg, OH) followed by well counter measurements of extracted myocardial tissue samples.

MATERIALS AND METHODS

Two dogs weighing approximately 25 kg each were used in the experiments. Technetium-99m-labeled macro-aggregated albumin (MAA) was administered through a catheter into the left ventricle. A sequential transmission/emission acquisition method was used (*22*). Before injecting ^{99m}Tc-labeled MAA into the left ventricle, a transmission scan using a line source and an FB collimator was performed to generate nonuniform attenuation maps of the canine thorax. An emission scan with two energy windows was acquired after the TCT scans. Figure 1 shows the TCT-SPECT acquisition system. Images were reconstructed using a filtered backprojection algorithm. Scatter correction was performed by using a dual-window scatter subtraction method (*23*). Attenuation compensation was performed by using Chang's attenuation correction method with one iteration (*3*). The measured mean counts from the SPECT images were converted to radionuclide concentrations (MBq/g) using a standard point source calibration and were com-

Received Feb. 16, 1994; revision accepted Jul. 21, 1994.

For correspondence or reprints contact: Ronald J. Jaszczak, PhD, Box 3949, Dept. of Radiology, Duke University Medical Center, Durham, NC 27710.

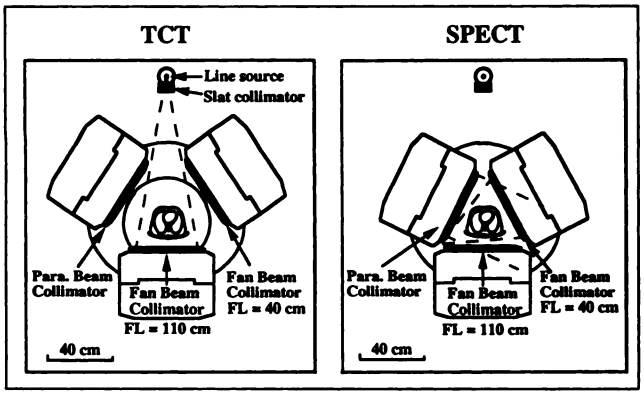

FIGURE 1. TCT-SPECT acquisition system.

pared with those of myocardial tissue samples obtained using the well counter.

TCT Data Acquisition

The TCT data acquisition system consisted of a line source, a slat collimator and a long focal length FB collimator (*22*), as indicated in Figure 1. The line source assembly had a 27-cm long stainless steel tube (1.0 mm inside diameter). In the first dog study, the tube was filled with 1139 MBq (30.8 mCi) of ^{99m}Tc. In the second dog study, the tube was filled with 2364 MBq (63.9 mCi) of ^{99m}Tc. The long focal length FB collimator (Nuclear Fields, Inc., Des Plaines, IL) had a focal length of 110 cm and was mounted on the scintillation camera opposite the line source. The FB collimator had a rectangular field of view (FOV) of 45.6 cm × 22.8 cm at the crystal surface. This FB collimator was used to provide collimation for the transmission gamma rays. Because of the poorer spatial resolution, this long focal length FB was not used for SPECT acquisitions.

The dogs were anesthetized with pentobarbital sodium (30 mg/kg intravenously) and were positioned in the gantry using an initial TCT scan to optimize the x, y and z positioning of the chest and the radius of rotation of the detection system. The radii of rotation for the two dog studies were 13.5 cm and 15 cm measured from the front surface of the collimator. The dogs were marked based on reference laser lights and were then removed. The TCT reference (in air) images were acquired into three non-rotational frames (250 sec/frame). Upon finishing the reference image acquisition, the dogs were repositioned in the scanner and realigned using the reference laser lights. TCT scans were performed of the chest. The TCT acquisition matrix was 128 × 64 × 180 angular views over 360°. The transaxial and axial linear sampling intervals were equal to 3.6 mm. Total scan time in both experiments was 15 min.

SPECT Data Acquisition

Upon finishing TCT scanning, ^{99m}Tc-labeled MAA was administered through the catheter into the left ventricle of each dog. A total of 462 MBq (12.5 mCi) was used for the first dog and 555 MBq (15.0 mCi) was used for the second dog. Emission scans with two energy windows (primary and scatter) were acquired. A primary energy window (130 keV ≤ Eγ ≤ 151 keV) and a scatter energy window (89 keV ≤ Eγ ≤ 127 keV) were used for the SPECT emission scans. Both a short focal length FB collimator (40 cm measured from the front surface of the collimator) and a low-energy super-high resolution (LESR) or a low-energy ultra-high resolution (LEUR) PB collimator were used. All collimators had a rectangular FOV of 45.6 cm × 22.8 cm at the crystal surface. The FB collimator had very high resolution and relatively low sensitivity (6 mm FWHM and 45 cps/MBq, respectively, at 14 cm from the collimator surface). The resolution (at 14 cm from the collimator surface) and sensitivity of the LESR collimator were 7 mm (FWHM) and 32 cps/MBq, respectively. The resolution (at 14 cm from the collimator surface) and sensitivity of the LEUR collimator were 9 mm (FWHM) and 57 cps/MBq, respectively. The SPECT acquisition matrix was 128 × 64 × 120 angular views over 360°. The linear sampling was 3.6 mm in both transaxial and axial directions. Total scan time in both experiments was 30 min.

Sample Measurements

Following the SPECT scans, the dogs were killed and the hearts were removed. Balloon catheters were inserted into the left ventricles of the hearts and were inflated using air. The hearts and balloon catheters were frozen using liquid nitrogen while air was continuously pumped into the heart to compensate for temperature-induced shrinkage of the balloon portion of the catheter. The hearts were then partially thawed and two mid-ventricle slices from each of the hearts were obtained in an anatomic axis (short-axis). Two thin methyl-methacrylate sheets (~1 mm) were used to slightly compress the heart slices to make them more uniform in thickness. The thickness of the slices was about 1.2 cm. For comparison purposes, high-resolution planar scans of the four heart slices were acquired by placing them directly on the surface of the collimator. After the planar scans, four samples from each of the four slices were obtained and weighed. Figure 2 illustrates the positions where the samples were taken in the first dog experiments. The positions were similar in the second dog experiment. These samples weighed from 0.6 g to 3.6 g. The activities of the 16 samples, together with two standard point sources (0.16 MBq in the first dog experiment and 0.36 MBq in the second dog experiment), were then measured using the planar gamma camera and a well counter. The measurements of the standard sources were used to generate the calibration factors (cps/MBq) for FB, LESR PB and LEUR PB collimators and the well counter.

Image Reconstruction

TCT data were reconstructed using a filtered backprojection (FBP) algorithm. The measured transmission data were converted to line integrals of linear attenuation by taking the natural logarithm of the ratio of the incident reference image to the measured

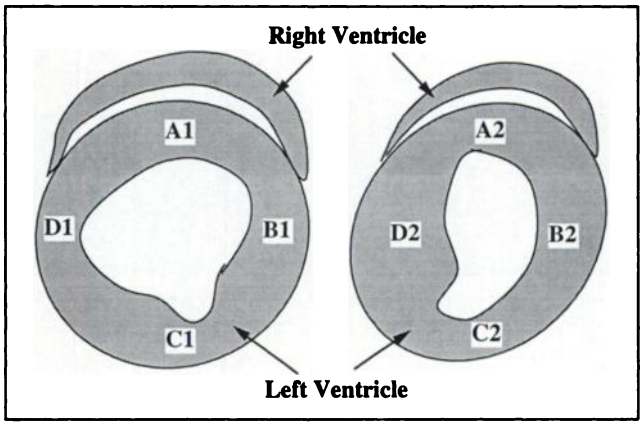

FIGURE 2. Two slices of the canine myocardium. A1-D1 and A2-D2 indicate the positions where the samples were taken.

TCT data. An 128 × 128 × 30-slice reconstruction matrix was used, which corresponds to a 3.6-mm pixel size and 3.6-mm slice thickness. A generalized Hann filter with a cutoff frequency of 0.85 cycles/cm was used for the TCT reconstruction. The nonuniform attenuation maps of the dog thorax were generated by using the TCT reconstructions. This TCT reconstruction also created a body contour. By assigning a constant attenuation coefficient (μ = 0.152 cm^{-1}) inside the body contour, we generated uniform attenuation maps. Figure 3 shows one slice of the uniform and the nonuniform attenuation map of the second dog thorax.

SPECT data were reconstructed using a FBP algorithm with scatter subtraction and single iteration Chang attenuation compensation. This algorithm was verified using a standard point source, both in air and in a 19-cm diameter and 15-cm long cylinder water bath before the dog study. The determined point source activity (region of interest (ROI): 60 pixels by 60 pixels, which encompassed the water bath) from the reconstructions was in good agreement with the source activity (5% error in both FB and PB reconstructions). The projections of the dog were precorrected for scatter. The dual-window subtraction method was used (*23*). The scatter subtraction constant k was experimentally determined using the above point source experiment. A dog-size cylinder was used. The photopeak window was 15%, which was the same as the one used in the dog studies. The scatter subtraction constant k was found to be 0.4. Chang's attenuation correction method with one iteration was used to compensate for the attenuation (*3*). Reconstructions with three types of attenuation compensation were performed: (1) without attenuation compensation; (2) with uniform attenuation compensation (μ = 0.152 cm^{-1}); and (3) with nonuniform attenuation compensation. An 128 × 128 × 30-slice reconstruction matrix was used. Generalized Hann filters with cutoff frequencies of 1.78 cycles/cm and 1.05 cycles/cm were used for the FB and PB SPECT reconstructions, respectively. These cutoff frequencies corresponded to 0.75 times the Nyquest frequencies of the FB (for the plane located at the center of rotation) and PB collimators, respectively. To compare the high-resolution FB reconstructions with the slightly lower-resolution LESR PB reconstructions, an additional FB image was reconstructed using the data of the first dog study. In this FB reconstruction, a generalized Hann filter with cutoff frequency (for the plane located at the center of rotation) of 1.05 cycles/cm was used, which was equal to 0.75 times the cutoff frequency for LESR PB reconstruction.

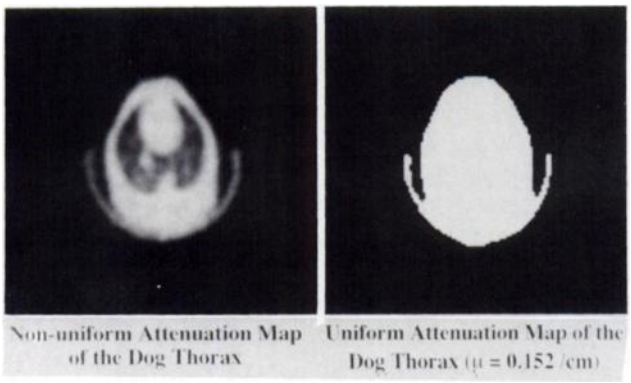

FIGURE 3. One slice of the uniform and nonuniform attenuation map of the canine thorax. The nonuniform attenuation map was generated using TCT scans and the uniform attenuation map was generated using the body contour with a constant attenuation coefficient.

Registration

To quantitatively evaluate the SPECT reconstructions, the images had to be registered to the planar images of the sliced heart, where the sample locations are known. The reconstructed images of the dog heart were re-oriented into a short-axis presentation. To match the thickness of the heart slices, three slices of the reconstructed SPECT images were added together to produce a final slice whose thickness was 1.1 cm. Figure 4 shows an example of the short-axis view SPECT image together with a high-resolution planar image of the sliced heart. Using the planar images of the sliced heart as a guide, the locations of the samples were determined in the re-oriented SPECT images. Since the locations may not correlate to the sample positions exactly, a moderately large ROI (2 pixel × 2 pixel or 0.7 cm × 0.7 cm) was used to measure the mean counts of these 16 sample locations. These mean counts were converted to radionuclide concentrations (MBq/g) using a standard source calibration, and were compared with those obtained using the well counter.

Statistical Analysis

With the 16 samples in this study, a statistical analysis was performed to get some indications of what the biases were between different reconstruction methods and the gold standard. A random block statistical model (*31*) was used, with the dogs taken to be the blocks. This model relies on two main assumptions. First, the response variance does not exhibit systematic variation from site-to-site. Second, the observations (and particularly the variation contribution from dog to dog) come from a normal distribution. The response variable in our case was $S/W - 1$, where S was the concentration in the ROI and W was the corresponding well counter measurement. Formally the model says that the response variable, y_{ij}, may be represented as

$$y_{ij} = \mu + d_i + \varepsilon_{ij},$$

where μ is an unknown constant, d_i is a random contribution due to the particular dog and ε_{ij} is an error term for the j-th measurement on the i-th dog. The random variable d_i is taken to be normally distributed with mean 0 and variance σ_d^2, and the random variable ε_{ij} is taken to be normally distributed with mean 0 and variance σ_e^2. The quantity of most interest is μ, the expected value of y_{ij}, which measures the approximate bias of the method. For balanced data, that is the same number of sites per dog, the estimate of μ is $\sum y_{ij}/n$, where n is the number of measurements. The variance of this estimate for the case of two dogs and eight

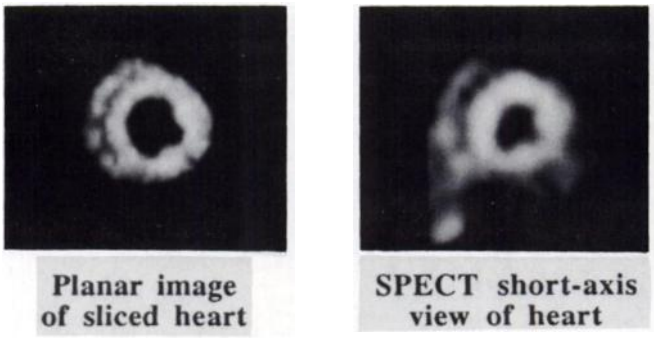

FIGURE 4. A short-axis view SPECT image and a planar image of the sliced heart.

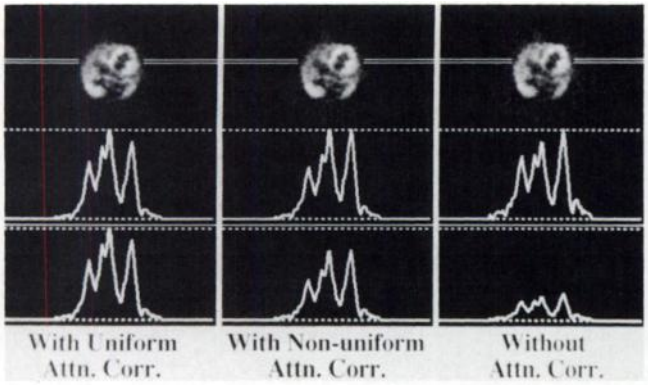

FIGURE 5. Transverse sectional images and profiles of the first dog heart using FB collimation.

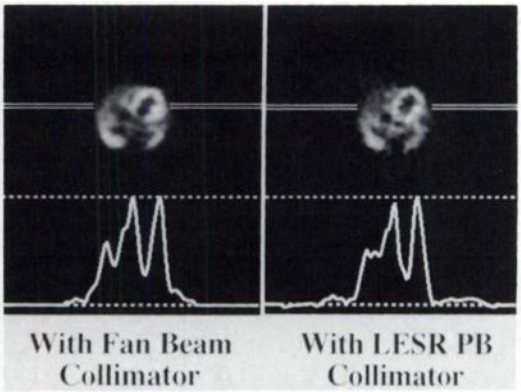

FIGURE 7. Comparison of the FB reconstruction with the LESR PB reconstruction. Note that the same filter was used in both reconstructions.

sites per dog will be $(8\sigma_d^2 + \sigma_e^2)/16$. The estimate for σ_d^2 will have a scaled chi-square distribution (with degrees of freedom 1 for the case of two dogs), and the estimate for σ_e^2 will also have a scaled chi-square distribution (with 14 degrees of freedom for the case of 16 sites). However, the sum of the two estimates will not in general have a chi-square distribution because they use different scale factors. This being the case, the usual Student's t-test must be applied with some care. If σ_d^2 dominates, the test acts as though it had 1 degree of freedom. If σ_e^2 dominates, the test acts as though it had 14 degrees of freedom. In general, the test will behave approximately as though it had a degrees of freedom value intermediate between these two values.

RESULTS

The transverse sectional images and profiles of the first dog heart using FB and LESR PB collimators are shown in Figures 5 and 6, respectively. The images were single-slice images 3.6 mm thick. In both figures, the bottom row shows the profiles with the fixed scale. All the FB reconstructions demonstrate similar quality to each other, and all the PB reconstructions demonstrate similar quality to each other as well. The right ventricle in FB reconstructions is more clearly visualized compared with that in LESR PB reconstructions. However, this may result partially from the higher cutoff frequency used in FB reconstructions.

To minimize the influence of the filter on the images, the additional FB reconstruction is compared with the LESR PB reconstruction in Figure 7. Note that both reconstructions used the same cutoff frequency. The right ventricle in FB reconstructions is still better defined and more clearly visualized compared with that in LESR PB reconstructions. The FB reconstruction is also less noisier than the LESR PB reconstruction.

The transverse sectional images and profiles of the second dog heart using FB and LEUR PB collimators are shown in Figures 8 and 9, respectively. Note that during the injection of ^{99m}Tc-MAA, the right ventricle preferentially received radioactivity, probably related to the catheter location directing activity into the right coronary artery. The images have to be windowed to clearly show the left ventricle. Gray bars have been added to indicate the lower display intensity used. Again, images in each group are judged to have a similar quality.

The concentrations (MBq/g) determined from the three types of SPECT reconstructions using FB and PB, as well as the well counter measurements and the gamma camera measurements are tabulated in four tables. The results of

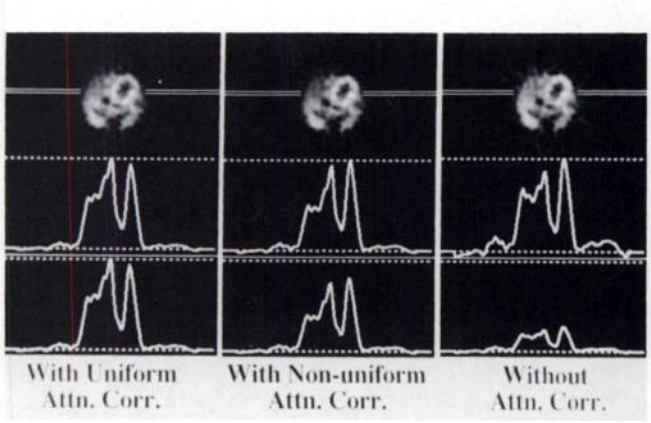

FIGURE 6. Transverse sectional images and profiles of the first dog heart using LESR PB collimation.

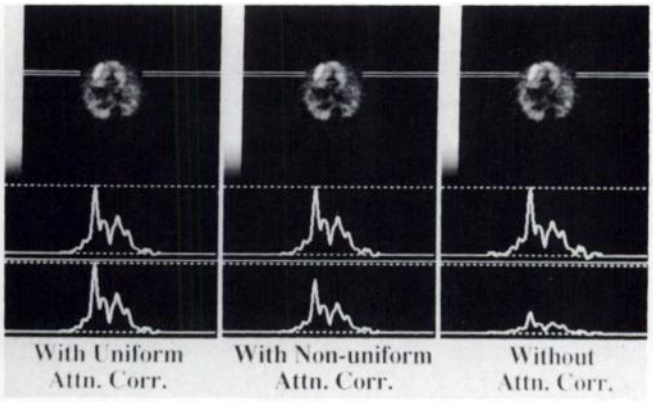

FIGURE 8. Transverse sectional images and profiles of the second dog heart using FB collimation. The images have been windowed to show the left ventricle.

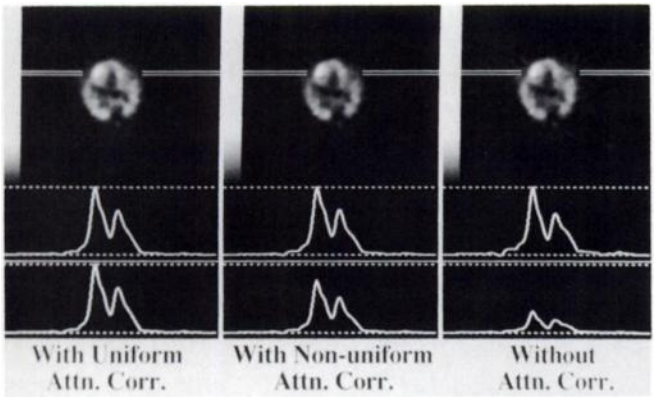

FIGURE 9. Transverse sectional images and profiles of the second dog heart using LEUR PB collimation. The images have been windowed to show the left ventricle.

TABLE 2
In Vivo Quantification of Canine Myocardial Radioactivity of Dog No. 1 Using LESR PB Collimator

	Concentration (MBq/g)				
Sample	Without attenuation correction	With uniform attenuation correction	With nonuniform attenuation correction	Gamma camera measurement	Well counter measurement
A1	0.027	0.106	0.082	0.084	0.079
B1	0.029	0.103	0.085	0.091	0.084
C1	0.032	0.113	0.093	0.095	0.098
D1	0.033	0.146	0.098	0.107	0.111
A2	0.035	0.133	0.110	0.109	0.114
B2	0.032	0.112	0.098	0.095	0.104
C2	0.033	0.139	0.106	0.105	0.103
D2	0.022	0.098	0.073	0.080	0.078

the first dog experiment are listed in Tables 1 and 2 for FB and LESR PB collimation, respectively. The results of the second dog experiment are listed in Tables 3 and 4 for FB and LEUR PB collimation, respectively. In all tables, the well counter measurements are listed in the last column. The comparisons demonstrate that with nonuniform attenuation correction, the concentrations are determined fairly accurately using both FB and PB reconstructions, with the maximum error less than 13%, although the LEUR PB results seem to be systematically 6% lower than the well counter measurements. The concentrations are over-estimated in SPECT reconstructions with uniform attenuation correction (8%–40% errors), and under-estimated without attenuation correction (~65% errors).

The above results demonstrated the accuracy of different reconstruction methods. It is also of general interest to know the precision of different reconstruction methods. To compare the precision, we first need to remove the bias. A scale factor was found for each of the reconstruction methods based on the mean value of the SPECT concentration measurements and the mean value of the well counter measurements. The SPECT measurements were then multiplied by the corresponding scaling factors. The scaled concentrations are listed in Tables 5–8. The percentage fractional differences between these scaled concentrations and the well counter measurements are also calculated and listed in parentheses. The percentage fractional difference is defined as the difference between the scaled concentration and the well counter measurement divided by the well counter measurement times 100. The comparison indicates that all the reconstruction methods have approximately the same range of fluctuation in concentration measurement.

To statistically model the measured concentrations, the MIXED procedure in the SAS software system (*32*) was used to fit the random block models. An approximate 95% confidence interval $[\bar{x} - t_0 S; \bar{x} + t_0 S]$ for μ (the bias) was calculated for different reconstruction methods and different collimators, where $\bar{x}$ is the estimate for μ, t_0 is a critical value from the t distribution and S is the estimate standard error of $\bar{x}$. The degrees of freedom used for the critical value t_0 were determined based on the values of the estimates of σ_d^2 and σ_e^2, which were determined by the fitting.

TABLE 1
In Vivo Quantification of Canine Myocardial Radioactivity of Dog No. 1 Using Fanbeam Collimator

	Concentration (MBq/g)				
Sample	Without attenuation correction	With uniform attenuation correction	With nonuniform attenuation correction	Gamma camera measurement	Well counter measurement
A1	0.029	0.100	0.086	0.084	0.079
B1	0.034	0.109	0.087	0.091	0.084
C1	0.034	0.113	0.098	0.095	0.098
D1	0.033	0.137	0.099	0.107	0.111
A2	0.033	0.128	0.116	0.109	0.114
B2	0.033	0.120	0.105	0.095	0.104
C2	0.033	0.118	0.095	0.105	0.103
D2	0.028	0.108	0.080	0.080	0.078

TABLE 3
In Vivo Quantification of Canine Myocardial Radioactivity of Dog No. 2 Using FB Collimator

	Concentration (MBq/g)				
Sample	Without attenuation correction	With uniform attenuation correction	With nonuniform attenuation correction	Gamma camera measurement	Well counter measurement
A1	0.065	0.217	0.186	—*	0.183
B1	0.057	0.186	0.155	0.152	0.160
C1	0.049	0.174	0.131	0.127	0.124
D1	0.050	0.148	0.127	0.131	0.122
A2	0.058	0.205	0.164	0.154	0.149
B2	0.075	0.239	0.180	0.199	0.188
C2	0.053	0.166	0.135	0.118	0.129
D2	0.053	0.196	0.147	0.154	0.152

* Sample was positioned outside the camera field of view.

TABLE 4
In Vivo Quantification of Canine Myocardial Radioactivity of Dog No. 2 Using LEUR PB Collimator

	Concentration (MBq/g)				
Sample	Without attenuation correction	With uniform attenuation correction	With nonuniform attenuation correction	Gamma camera measurement	Well counter measurement
A1	0.061	0.204	0.172	—*	0.183
B1	0.058	0.182	0.152	0.152	0.160
C1	0.043	0.146	0.119	0.127	0.124
D1	0.035	0.144	0.108	0.131	0.122
A2	0.053	0.163	0.148	0.154	0.149
B2	0.065	0.224	0.172	0.199	0.188
C2	0.044	0.177	0.124	0.118	0.129
D2	0.045	0.179	0.132	0.154	0.152

* Sample was positioned outside the camera field-of-view.

Approximations for the degrees of freedom can be obtained by matching the first two moments of the distribution (*33*). For the case of no attenuation correction, the estimate of σ_d^2 was comparable to the estimate of σ_e^2. This suggested that the critical values for the confidence intervals should come from a t distribution with one degree of freedom. The critical value is 12.7. For the other response variables, the estimate of σ_d^2 was much smaller than the estimate of σ_e^2, and a critical value of 2.25 was chosen for 95% confidence corresponding to 10° of freedom. It is notable that the estimate of the component of variability due to dog-specific effects was reduced for methods that attempt dog-specific attenuation correction. The results for the FB and PB collimators are given in Tables 9 and 10, respectively. The small estimated μ values ($\leq$5%) for the nonuniform attenuation correction method demonstrated that the concentrations were most accurately determined in FB and PB SPECT reconstructions with nonuniform attenuation compensation. The fact that there is no overlap between the 95% confidence intervals for nonuniform attenuation compensation and uniform attenuation compensation or for nonuniform attenuation compensation and without attenuation compensation indicated the statistical significance of the differences among different attenuation correction methods. However, we admit that with only two dogs in our sample, we are relying strongly on our modeling assumptions.

DISCUSSION

One of the most utilized clinical applications of SPECT is cardiac imaging. We have demonstrated that with nonuniform attenuation correction and scatter subtraction, the concentrations of a ^{99m}Tc radiopharmaceutical within the canine myocardium could be accurately determined. Both FB and PB SPECT reconstructions produced similar quantitative results. However, for several reasons, the conclusions are not intended to be extended to human patient studies directly. First, in the dog study, ^{99m}Tc-MAA was injected directly into the left ventricle. This approach is not clinically feasible because radiopharmaceuticals for imaging the myocardium are injected intravenously in clinical studies. The concentration of the radiopharmaceuticals in the myocardium will be much lower and images will be noisier, which may affect the accurate determination of the concentrations. Second, the dogs used in this study are smaller than a normal adult patient. In patient studies, especially in studies of large patients, truncation may occur during the TCT scans using a line source and currently available TCT FB collimators. Although the truncated TCT images may still provide fairly accurate attenuation coefficients for regions inside the field of view (*16*), the truncation effect on the SPECT quantification still needs to be evaluated. Also due to the larger size of an adult patient, a larger radius of rotation is required, thus the heart is further away from the detector. The longer distance of the

TABLE 5
Comparison of Precision of Different Reconstruction Methods Using Scaled Concentrations of Dog No. 1 Obtained Using a FB Collimator

	Scaled Concentration (MBq/g)				
Sample	Without attenuation correction	With uniform attenuation correction	With nonuniform attenuation correction	Gamma camera measurement	Well counter measurement
A1	0.087 (10%)*	0.083 (5%)	0.087 (10%)	0.085 (7%)	0.079
B1	0.102 (21%)	0.090 (7%)	0.088 (5%)	0.092 (9%)	0.084
C1	0.102 (4%)	0.093 (−5%)	0.099 (1%)	0.096 (−2%)	0.098
D1	0.099 (−11%)	0.113 (2%)	0.100 (−10%)	0.108 (−3%)	0.111
A2	0.099 (−13%)	0.106 (−7%)	0.117 (3%)	0.110 (−4%)	0.114
B2	0.099 (−5%)	0.099 (−5%)	0.106 (1%)	0.096 (−8%)	0.104
C2	0.099 (−4%)	0.097 (−6%)	0.096 (−7%)	0.106 (3%)	0.103
D2	0.084 (8%)	0.089 (14%)	0.081 (4%)	0.081 (3%)	0.078

* Percentage fractional differences between SPECT and planar measurements and the well counter measurements. The listed measurements have been scaled to remove the bias.

TABLE 6
Comparison of Precision of Different Reconstruction Methods Using Scaled Concentrations of Dog No. 1 Using a LESR PB Collimator

Sample	Scaled Concentration (MBq/g)				
	Without attenuation correction	With uniform attenuation correction	With nonuniform attenuation correction	Gamma camera measurement	Well counter measurement
A1	0.086 (9%)*	0.086 (9%)	0.085 (8%)	0.085 (7%)	0.079
B1	0.092 (10%)	0.084 (0%)	0.088 (5%)	0.092 (9%)	0.084
C1	0.102 (4%)	0.092 (−6%)	0.096 (−2%)	0.096 (−2%)	0.098
D1	0.105 (−5%)	0.118 (6%)	0.101 (−9%)	0.108 (−3%)	0.111
A2	0.111 (−3%)	0.108 (−5%)	0.114 (0%)	0.110 (−4%)	0.114
B2	0.102 (−2%)	0.091 (−13%)	0.101 (3%)	0.096 (−8%)	0.104
C2	0.105 (2%)	0.113 (10%)	0.108 (5%)	0.106 (3%)	0.103
D2	0.070 (−10%)	0.080 (3%)	0.076 (−3%)	0.081 (3%)	0.078

* Percentage fractional differences between SPECT and planar measurements and the well counter measurements. The listed measurements have been scaled to remove the bias.

heart from the detector may degrade the image resolution. The larger body size of an adult patient also means more scatter and attenuation for the heart. All these factors will make the quantification of the radiopharmaceutical distribution in human myocardium more difficult. However, this study does provide a good preclinical laboratory situation to evaluate the ability of SPECT to perform in vivo quantification using a dog model.

We compared different attenuation correction methods (without attenuation correction, with uniform and nonuniform attenuation correction). Differences were found among different attenuation correction methods. A statistical analysis was performed using the 16 samples obtained from the two dogs. The differences were found to be statistically significant using a random block model. However, due to the small number of dogs used, this model is quite sensitive to our model assumptions. More dog studies would be required to ensure that our model assumptions are completely valid.

We used ^{99m}Tc-MAA as myocardial perfusion tracer to optimize the myocardial accumulation and to minimize surrounding tissue accumulation. This model does not accurately simulate the distribution of ^{99m}Tc myocardial perfusion agents that are presently used. Furthermore, because of the particulate nature of ^{99m}Tc-MAA and the gradient of blood flow from epicardium to the endocardium, the endocardial-to-epicardial gradient of ^{99m}Tc-MAA may be different from other ^{99m}Tc myocardial perfusion tracers. However, because of the resolution of SPECT that results in a FWHM of 6–9 mm for these studies, the endocardial radioactivity cannot be accurately separated from the epicardial radioactivity. Therefore, the concentration of radioactivity in the entire thickness of the myocardium was compared using the SPECT data and the excised myocardium.

This study demonstrated the effects of the finite system resolution and sensitivity on reconstructed images and quantification. The FB collimator had the highest resolu-

TABLE 7
Comparison of Precision of Different Reconstruction Methods Using Scaled Concentrations of Dog No. 2 Using a FB Collimator

Sample	Scaled Concentration (MBq/g)				
	Without attenuation correction	With uniform attenuation correction	With nonuniform attenuation correction	Gamma camera measurement	Well counter measurement
A1	0.171 (−7%)*	0.171 (−7%)	0.183 (0%)	—†	0.183
B1	0.150 (−6%)	0.147 (−8%)	0.153 (−4%)	0.150 (−6%)	0.160
C1	0.127 (2%)	0.137 (10%)	0.129 (4%)	0.126 (2%)	0.124
D1	0.131 (7%)	0.117 (−4%)	0.125 (2%)	0.130 (7%)	0.122
A2	0.152 (2%)	0.162 (9%)	0.162 (9%)	0.152 (3%)	0.149
B2	0.197 (5%)	0.188 (0%)	0.177 (−6%)	0.197 (5%)	0.188
C2	0.139 (8%)	0.131 (2%)	0.133 (2%)	0.117 (−9%)	0.129
D2	0.139 (−8%)	0.155 (2%)	0.145 (−5%)	0.152 (0%)	0.152

* Percentage fractional differences between SPECT and planar measurements and the well counter measurements. The listed measurements have been scaled to remove the bias.
† Sample was positioned outside the camera field of view.

TABLE 8
Comparison of Precision of Different Reconstruction Methods Using Scaled Concentrations of Dog No. 2 Using a LEUR PB Collimator

Sample	Scaled Concentration (MBq/g)				
	Without attenuation correction	With uniform attenuation correction	With nonuniform attenuation correction	Gamma camera measurement	Well counter measurement
A1	0.182 (−1%)*	0.174 (−5%)	0.184 (1%)	—†	0.183
B1	0.173 (8%)	0.155 (−3%)	0.163 (2%)	0.150 (−6%)	0.160
C1	0.128 (3%)	0.124 (0%)	0.127 (2%)	0.126 (2%)	0.124
D1	0.105 (−14%)	0.122 (0%)	0.116 (−5%)	0.130 (7%)	0.122
A2	0.158 (6%)	0.139 (−7%)	0.159 (7%)	0.152 (3%)	0.149
B2	0.194 (3%)	0.191 (2%)	0.184 (−2%)	0.197 (5%)	0.188
C2	0.131 (2%)	0.151 (17%)	0.133 (3%)	0.117 (−9%)	0.129
D2	0.134 (−12%)	0.152 (0%)	0.141 (−7%)	0.152 (0%)	0.152

* Percentage fractional differences between SPECT and planar measurements and the well counter measurements. The listed measurements have been scaled to remove the bias.
† Sample was positioned outside the camera field of view.

tion and moderately high sensitivity (6 mm FWHM and 45 cps/MBq at 14 cm from the collimator surface, respectively). The LESR PB collimator had lower resolution and sensitivity (7 mm FWHM and 32 cps/MBq at 14 cm from the collimator surface). The wall thicknesses of the left ventricle and right ventricle were about 14 mm and 7 mm, respectively. These wall thicknesses were obtained from the sliced dog heart. The resolution became important with the object as small as the dog's ventricles. As demonstrated in Figure 7, we were able to show the higher quality heart images of FB collimation compared with those of lower resolution and sensitivity LESR PB collimation with the use of the same filter. The right ventricle in FB reconstructions was better defined and more clearly visualized and the images were less noisy. With LEUR PB (9 mm FWHM at 14 cm from the collimator surface) results, we believe that the finite resolution effect (*34–36*) may also partially explain the fact that the LEUR PB results obtained with nonuniform attenuation compensation were systematically 6% lower than the well counter measurements. Another factor which may degrade the image quality is heart motion. In this study, gating was not used. Gated cardiac studies can minimize the effect of myocardial motion. However, the counts per frame will be lower and images will be noisier than for nongated images. Future research is required to investigate the loss in image quality resulting from the cardiac motion and to find out whether better quantification can be obtained using cardiac gating. A beating heart phantom has been recently developed in our laboratory (*37*) and in the near future, we will be able to perform gated and nongated studies with both high and low radionuclide concentrations.

In this study, the nonuniform attenuation map of the dog thorax was generated using a collimated line source and a long focal length FB collimator. High-quality TCT reconstructions were obtained using this technique to provide an accurate attenuation map for SPECT reconstructions. The uniform attenuation map was generated using the body contour and the attenuation coefficient of water ($\mu = 0.152$ cm^{-1}) was assigned inside the body contour. As demonstrated in Figures 5, 6, 8 and 9, qualitatively, the images obtained with uniform and nonuniform attenuation corrections are similar for this relatively small object. The qualitative similarity between the results for uniform and nonuniform attenuation may have something to do with the small size of the canine thorax. In patient studies, especially in large patients the finding may be different. Quantitatively, however, the use of the uniform attenuation correction causes the over-estimation of the concentrations. If only the quantification of myocardium is desired, this overestimation of the concentrations with uniform attenuation compensation may be reduced by using an empirically

TABLE 9
Approximate 95% Confidence Intervals for Estimate (μ) of Different Reconstruction Methods Using a FB Collimator

Reconstruction method	Estimate (μ)	Critical Value	95% Confidence Interval
Without attn. corr.	−0.64	12.7	(−0.93; −0.35)
With uniform attn. corr.	0.25	2.25	(0.19; 0.31)
With nonuniform attn. corr.	0.01	2.25	(−0.02; 0.04)

TABLE 10
Approximate 95% Confidence Intervals for Estimate (μ) of Different Reconstruction Methods Using a PB Collimator

Reconstruction method	Estimate (μ)	Critical value	95% Confidence interval
Without attn. corr.	−0.68	12.7	(−0.79; −0.56)
With uniform attn. corr.	0.21	2.25	(0.15; 0.27)
With nonuniform attn. corr.	−0.05	2.25	(−0.09; −0.01)

determined smaller value for the linear attenuation coefficient. However, this assumed smaller attenuation coefficient will be object-dependent and its optimal value would be difficult to determine for many imaging situations. Also this smaller attenuation coefficient does not reconstruct quantitative levels in other regions of the image, such as lungs.

In this study, scatter subtraction technique with a constant k was used. The constant k was determined by using a point source both in air and dog-size water bath. The value of k may not be the optimized value for the dog thorax geometry. However, because of the following reasons, the use of this constant should not introduce a large error in quantification of radiopharmaceutical distribution in canine myocardium. First, in this study the constant value k was found to be 0.4. This value is consistent with the value found by Gilland et al. (*14*), and close to the value of 0.5 given by Jaszczak et al. (*23*), although a different imaging system, energy window, source and phantom were used. These results suggest that k is not very sensitive to the attenuation distribution. Second, the accuracy of the reconstructed images is not sensitive to error in k. Studies have shown that a 25% error in k resulted in only less than 7% incremental error in the reconstruction (*14,23*).

ACKNOWLEDGMENTS

This work was supported by a PHS grant awarded by the National Cancer Institute and in part by a grant awarded by the Department of Energy.

REFERENCES

1. Kay DB, Keyes JW. First-order corrections for absorption and resolution compensation in radionuclide Fourier tomography. *J Nucl Med* 1975;16: 540–541.
2. Budinger TF, Derenzo SE, Gullberg GT, Greenberg WL, Huesman RH. Emission computed assisted tomography with single photon and positron annihilation photon emitters. *J Comput Assist Tomog* 1977;1:131–145.
3. Chang LT. A method for attenuation correction in radionuclide computed tomography. *IEEE Trans Nucl Sci* 1978;25:638–643.
4. Bellini S, Piacentini M, Cafforio C, Rocco F. Compensation of tissue absorption in emission tomography. *IEEE Trans Acoustics Speech Signal Proc* 1979;27:213–218.
5. Tretiak O, Metz CE. The exponential radon transform. *SIAM J Appl Math* 1980;39:341–354.
6. Tanaka E, Toyama H, Murayama HE. Convolutional image reconstruction for quantitative single photon emission computed tomography. *Phys Med Biol* 1984;29:1489–1500.
7. Gullberg GT, Huesman RH, Malko JA, Pelc NJ, Budinger TF. An attenuation projector-backprojector for iterative SPECT reconstruction. *Phys Med Biol* 1985;30:799–816.
8. Floyd CE, Jaszczak RJ, Greer KL, Coleman RE. Inverse Monte Carlo as a unified reconstruction algorithm for ECT. *J Nucl Med* 1986;27:1577–1585.
9. Malko JA, Van Heertum RL, Gullberg GT, Kowalsky WP. SPECT liver imaging using an iterative attenuation correction algorithm and an external flood source. *J Nucl Med* 1986;27:701–705.
10. Bailey DL, Hutton BF, Walker PJ. Improved SPECT using simultaneous emission and transmission tomography. *J Nucl Med* 1987;28:844–851.
11. Manglos SH, Jaszczak RJ, Floyd CE. Weighted backprojection implemented with a non-uniform attenuation map for improved SPECT quantification. *IEEE Trans Nucl Sci* 1988;35:625–628.
12. Manglos SH, Jaszczak RJ, Floyd CE, Hahn LJ, Greer KL, Coleman RE. A quantitative comparison of attenuation-weighted backprojection with multiplicative and iterative post-processing attenuation compensation in SPECT. *IEEE Trans Med Imag* 1988;7:127–134.
13. Tsui BMW, Gullberg GT, Edgerton ER, et al. Correction of nonuniform attenuation in cardiac SPECT imaging. *J Nucl Med* 1989;30:497–507.
14. Gilland DR, Jaszczak RJ, Greer KL, Coleman RE. Quantitative SPECT reconstruction of iodine-123 data. *J Nucl Med* 1991;32:527–533.
15. Manglos SH, Bassano DA, Thomas FD. Cone beam transmission computed tomography for nonuniform attenuation compensation of SPECT images. *J Nucl Med* 1991;32:1813–1820.
16. Tung CH, Gullberg GT, Zeng GL, Christian PE, Datz FL, Morgan HT. Nonuniform attenuation correction using simultaneous transmission and emission converging tomography. *IEEE Trans Nucl Sci* 1992;39:1134–1143.
17. Bailey DL, Eberl S, Tan P, Meikle SR, Fulton RR, Hutton BF. Implementation of a scanning line source for attenuation correction with simultaneous emission/transmission SPECT [Abstract]. *J Nucl Med* 1992;33:901.
18. Galt JR, Cullom SJ, Garcia EV. SPECT quantification: a simplified method of attenuation and scatter correction for cardiac imaging. *J Nucl Med* 1992;33:2232–2237.
19. Frey EC, Tsui BMW, Perry R. Simultaneous acquisition of emission and transmission data for improved thallium-201 cardiac SPECT using a technetium-99m transmission source. *J Nucl Med* 1992;33:2238–2245.
20. Greer KL, Harris CC, Jaszczak RJ, et al. Transmission computed tomography data acquisition with a SPECT system. *J Nucl Med Technol* 1987; 15:53–56.
21. Gilland DR, Jaszczak RJ, Turkington TG, Greer KL, Coleman RE. Transmission data acquisition with a three-headed SPECT system [Abstract]. *J Nucl Med* 1991;33:901.
22. Jaszczak RJ, Gilland DR, Hanson MW, Jang S, Greer KL, Coleman RE. Fast transmission CT for determining attenuation maps using a collimated line source, rotatable air-copper-lead attenuators and fanbeam collimation. *J Nucl Med* 1993;34:1577–1586.
23. Jaszczak RJ, Greer KL, Floyd CE, Harris CC, Coleman RE. Improved SPECT quantification using compensation for scattered photons. *J Nucl Med* 1984;25:893–900.
24. Yanch JC, Flower MA, Webb S. Improved quantification of radionuclide uptake using deconvolution and windowed subtraction techniques for scatter compensation in single photon emission computed tomography. *Med Phys* 1990;17:1011–1022.
25. Frey EC, Tsui BMW. Parameterization of the scatter response function in SPECT imaging using Monte Carlo simulation. *IEEE Trans Nucl Sci* 1990; 37:1308–1315.
26. Wang X, Koral KF. A regularized deconvolution-fitting method for Compton-scatter correction in SPECT. *IEEE Trans Med Imag* 1992;11:351–360.
27. King MA, Hademenos GJ, Click SJ. A dual-photopeak window method for scatter correction. *J Nucl Med* 1992;33:605–612.
28. Smith MF, Floyd CE, Jaszczak RJ, Coleman RE. Evaluation of projection pixel-dependent and pixel-independent scatter correction in SPECT. *IEEE Trans Nucl Sci* 1992;39:1099–1105.
29. Smith MF, Jaszczak RJ. Generalized dual-energy-window scatter compensation in spatially varying media for SPECT. *Phys Med Biol* 1994;39:531–546.
30. Ljungberg M, King MA, Hademenos GJ, Strand SE. Comparison of four scatter correction methods using Monte Carlo simulated source distributions. *J Nucl Med* 1994;35:143–151.
31. Searle SR, Casella G, McCulloch CE. *Variance components.* New York: Wiley; 1971:122–135.
32. SAS Institute Inc. *SAS technical report P229: SAS/STAT software: changes and enhancements* (release 1.07). Cary NC: SAS Institute Inc.; 1992.
33. Satterthwaite FE. An approximation distribution of estimates of variance components. *Biometries Bull* 1946;2:110–114.
34. Hoffman EJ, Huang S, Phelps ME. Quantitation in position emission computed tomography: I. effect of object size. *J Comput Assist Tomogr* 1979; 3:299–308.
35. Jaszczak RJ, Coleman RE, Whitehead FR. Physical factors affecting quantitative measurements using camera-based single photon emission computed tomography. *IEEE Trans Nucl Sci* 1981;28:68–80.
36. Karp JS, Daube-Witherspoon ME, Muehllehner G. Factors affecting accuracy and precision in PET volume imaging. *J Cereb Blood Flow Metab* 1991;11:A38–44.
37. Jang S, Jaszczak RJ, Li J, et al. Cardiac ejection fraction and volume measurements using dynamic cardiac phantoms and radionuclide imaging. *IEEE Trans Nucl Sci* 1994:in press.